2023 AIAA Aviation and Aeronautics Forum and Exposition (AIAA AVIATION Forum),
12-16 June 2023, San Diego, USA
DOI:10.2514/6.2023-4079

Aero-whisker for the Measurement of Aircraft Flight Speed and Angle of Attack in Compressible Flow Conditions

Marco Debiasi[1]
Cranfield University, Defence Academy of the UK, Shrivenham, SN6 8LA, United Kingdom
Corresponding author: marco.debiasi@cranfield.ac.uk

Kevin Atkinson[2]
Royal Navy, United Kingdom

Alistair Saddington[3]
Cranfield University, Defence Academy of the UK, Shrivenham, SN6 8LA, United Kingdom

Mark Finnis[4]
Cranfield University, Defence Academy of the UK, Shrivenham, SN6 8LA, United Kingdom

A whisker-like device has been designed and tested that simultaneously measures the speed and the direction of a flow in which it protrudes. The device consists of a thin cylindrical probe longer than the thickness of the local boundary layer whose aerodynamic drag produces a moment at its base which is measured by a solid-state torque transducer. With proper calibration, the orthogonal components of the moment can be used to measure the speed and the direction of the flow. Measurements have been performed in a wind tunnel to validate the design at flow velocities ranging from Mach 0.15 to Mach 0.87 and for flow angles relative to the probe ranging from -88° to +88°. The results obtained indicate that the aero-whisker is capable to accurately measure the Mach number and direction of the flow with potential for further optimization for aircraft applications.

I. Nomenclature

C_d	=	drag coefficient of a smooth, infinite-length, circular cylinder
d	=	drag per unit length of the probe's shaft
E	=	Young's modulus of the material of the probe's shaft
F	=	magnitude of the force at the top of the transducer
I	=	area moment of inertia of the probe's shaft section
L	=	length of the probe's shaft
L_b	=	thickness of the probe's base
M	=	Mach number measured by the aero-whisker
M_∞	=	freestream Mach number
r	=	radius of the probe's shaft

[1] Research Fellow, Aeromechanical Systems Group, Centre for Defence Engineering, AIAA Member.
[2] Air Engineer.
[3] Reader, Aeromechanical Systems Group, Centre for Defence Engineering.
[4] Principal Research Fellow, Aeromechanical Systems Group, Centre for Defence Engineering.

Re = Reynolds number
St = Strouhal number
t = time
T = magnitude of the moment at the top of the transducer
x = streamwise coordinate
y = spanwise coordinate

δ = displacement of the tip of the probe
μ = viscosity of the air
θ = flow angle measured by the aero-whisker
θ_∞ = freestream angle relative to the aero-whisker
ρ = density of the air

II. Introduction

The aim of this project was to investigate the feasibility of whisker-like devices to be used as sensors for simultaneous measurements of the airspeed and flow angle of an aircraft flying at subsonic conditions.

With few exceptions, the current approach to collect such data is to use relatively large air data probes placed in a few selected locations on an aircraft. In some cases, the size and weight of these devices cannot be reduced without compromising their performance. This and their cost prevent their application to small or very small vehicles such as autonomous unmanned aerial vehicles (UAVs) and micro air vehicles (MAVs). Since only a few such probes are installed on an aircraft, the malfunction of one of them can upset its control and lead to its catastrophic loss, an example of which was the failure of the pitot probes in the crash of Air France flight 447 (June 2009) [1] or of the angle-of-attack sensors in the crashes of Lion Air flight 610 (October 2018) [2] and Ethiopian Airlines flight 302 (March 2019) [3-5].

Solid-state transducers, on the other hand, continue to demonstrate increased performance and a decrease in size and cost. In particular, the piezoelectric, piezoresistive and semiconductor types are among the most robust, compact and reliable. In recent years they have been used to replace a vast array of sensors traditionally used for measuring pressure, force, and strain. Potentially they can be used to measure aerodynamic parameters directly, with a suitable design implementation.

For this, inspiration can be drawn from nature. Birds in flight sense the airflow around them largely by using their feathers, which transfer the aerodynamic forces to the innervated body areas to which they are attached. The highly evolved and varied structure of feathers challenges their artificial replication. Hair and whiskers (or vibrissae) are the mammalian sensing counterpart of feathers. Bats use tiny hairs on the surface of their wings to detect and adapt to changing airflow [6]. Whiskers are more specialized hairs with a much simpler structure than feathers. They are connected to hair follicles that are heavily innervated by sensory nerves, which allow some mammals to use them to finely probe their surroundings. Such sensory hair structure can be replicated by connecting a thin shaft to a solid-state transducer measuring the moments about three orthogonal axes. When bent by an external force the shaft induces a moment in the transducer whose magnitude and direction can be used to characterize the external force. Jiang et al. summarize the recent progress for this type of bio-inspired flow sensor [7]. Research in this area has mainly focused on creating MEMS sensors mimicking the hair of arthropods [8-19] or seal whiskers for underwater applications [20-23].

For aerodynamic applications, an element in the shape of a sphere (or another suitable shape) can be added to the tip of the shaft to stabilize and amplify the effect of the aerodynamic forces. The velocity and the direction of the flow producing the aerodynamic force can then be reconstructed from the signals of the solid-state transducer. This would allow the simultaneous measurement of the airspeed and of its direction relative to an aircraft. Thus, two parameters of vital importance for the ability of air crew to safely operate an aircraft can be measured by a single, simple, reliable, solid-state device with the potential of miniaturization and mass production. The latter might facilitate the implementation, even in small aircraft, of distributed sensor-rich systems providing more flight information than traditional sensors [24, 25]. The redundancy in these systems that supply both the airspeed and its direction and that, compared to traditional air data probes, have very different mechanisms for failure would prevent the total loss of available information in the case of failure of one or more duplicate sensors.

To validate the aero-whisker concept above, two initial prototypes were designed and tested in a low-speed wind tunnel at flow velocities up to 30 m/s [26]. The aero-whisker probe consisted of a shaft whose tip was terminated by a sphere and whose base was connected to a solid-state torque transducer. Once calibrated, the aero-whisker was

able to use the signals of the transducer to accurately reconstruct the velocity and the direction of the flow producing the aerodynamic drag of its probe. The current paper presents the results of a follow-on research project where the aero-whisker concept has been tested in a range of subsonic Mach numbers pertinent to the flight of commercial aircraft.

III. Aero-whisker Design

An aero-whisker comprises a probe and a solid-state force/torque transducer at its base. The probe is a circular shaft (tube or rod) that placed in an air flow generates aerodynamic drag whose force $\vec{F}$ and moment (torque) $\vec{T}$ at the bottom of the probe base are measured by the transducer, Fig. 1.

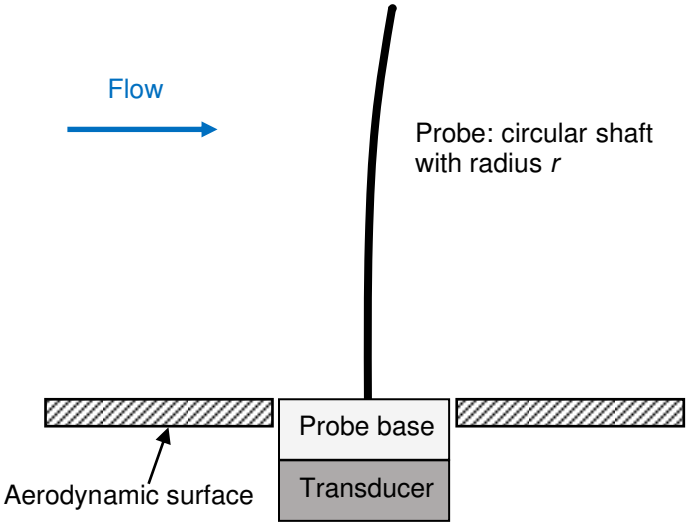

Fig. 1 Schematic of the aero-whisker setup.

If the boundary-layer thickness is small compared with the length L of the probe, the shaft can be modelled as a cantilever beam of length L with a distributed force d corresponding to the drag of a circular cylinder (drag per unit length), Fig. 2.

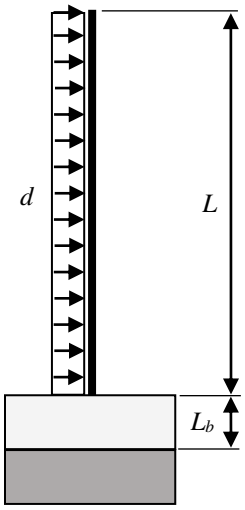

Fig. 2 Cantilever-beam model with distributed (drag) force.

The magnitude F of the force and T of the moment measured by the transducer and the displacement δ of the probe's tip in the flow direction can be calculated as:

$$F = dL \tag{1}$$

$$T = \frac{1}{2}dL^2 + FL_b \tag{2}$$

$$\delta = \frac{1}{8}\frac{dL^4}{EI} \tag{3}$$

where E is the Young's modulus of the shaft material and

$$I = \frac{\pi}{4}r^4 \tag{4}$$

is the area moment of inertia of the shaft section having external radius r. The drag d is obtained as:

$$d = \left(\frac{1}{2}\rho a^2 M_\infty^2\right) 2rC_d \tag{5}$$

where ρ and a are the density and speed of sound of the air, respectively, at the freestream Mach number M_∞ and C_d is the drag coefficient of a smooth, infinite-length, circular cylinder, Fig. 3.

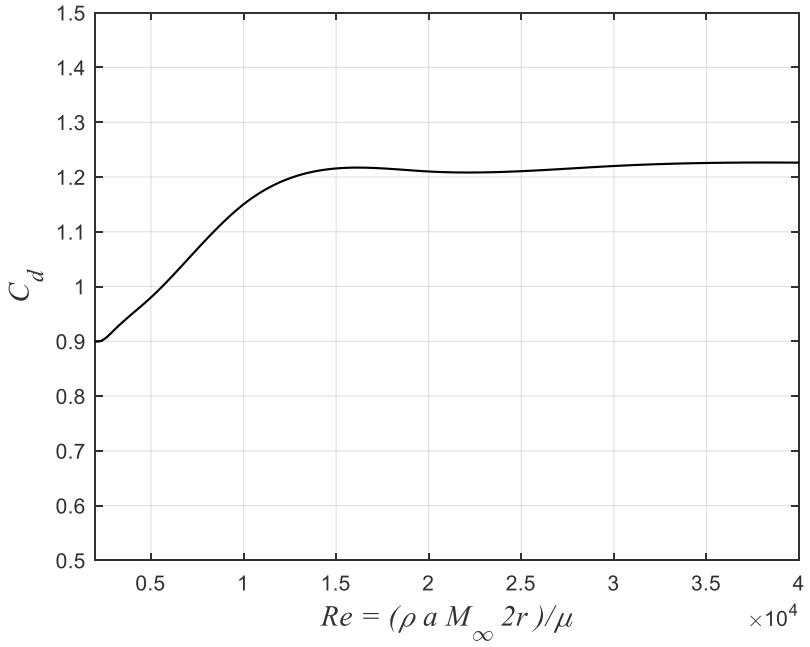

Fig. 3 Drag coefficient of a smooth, infinite-length, circular cylinder as a function of its Reynolds number in the range relevant to the current aero-whisker design (based on data from [27]).

IV. Experimental Setup

The probe was mounted on an ATI Mini 40 solid-state force/torque transducer capable of measuring the forces and torques (moments) along three perpendicular axes. The range (and resolution) of the force measurable along the x and y axes of the transducer aligned with the streamwise and spanwise directions of the wind-tunnel test section was 20.0 (±1/200) N. The range (and resolution) of the moment measurable along the same axes was 1.0 ($\pm 1/8 \cdot 10^{-3}$) N·m. The values of the force and moment were obtained from the sensor output using the factory-supplied calibration.

AISI 1080 steel was selected for fabricating the probe's shaft due to its combination of strength, elasticity and availability as standard diameter rods. Equations 1, 2 and 5 were used to predict the magnitude F of the force and T of the moment at the top of the transducer for different values of the length L and of the radius r of the shaft at freestream Mach numbers between 0.05 and 0.9 at standard, sea-level atmospheric conditions. The shaft radius should be minimized to increase its bending in the freestream direction [26]. However, this is limited by the maximum stress at the base of the shaft that should not exceed the tensile yield strength of its material. Calculations indicated that AISI 1080 shafts with radius r = 1 mm and length L up to 100 mm would not plastically deform in the range of Mach number explored. An aluminium probe's base with thickness L_b = 20 mm was selected to ensure a stable and secure insertion of the probe's shaft and connection to the transducer.

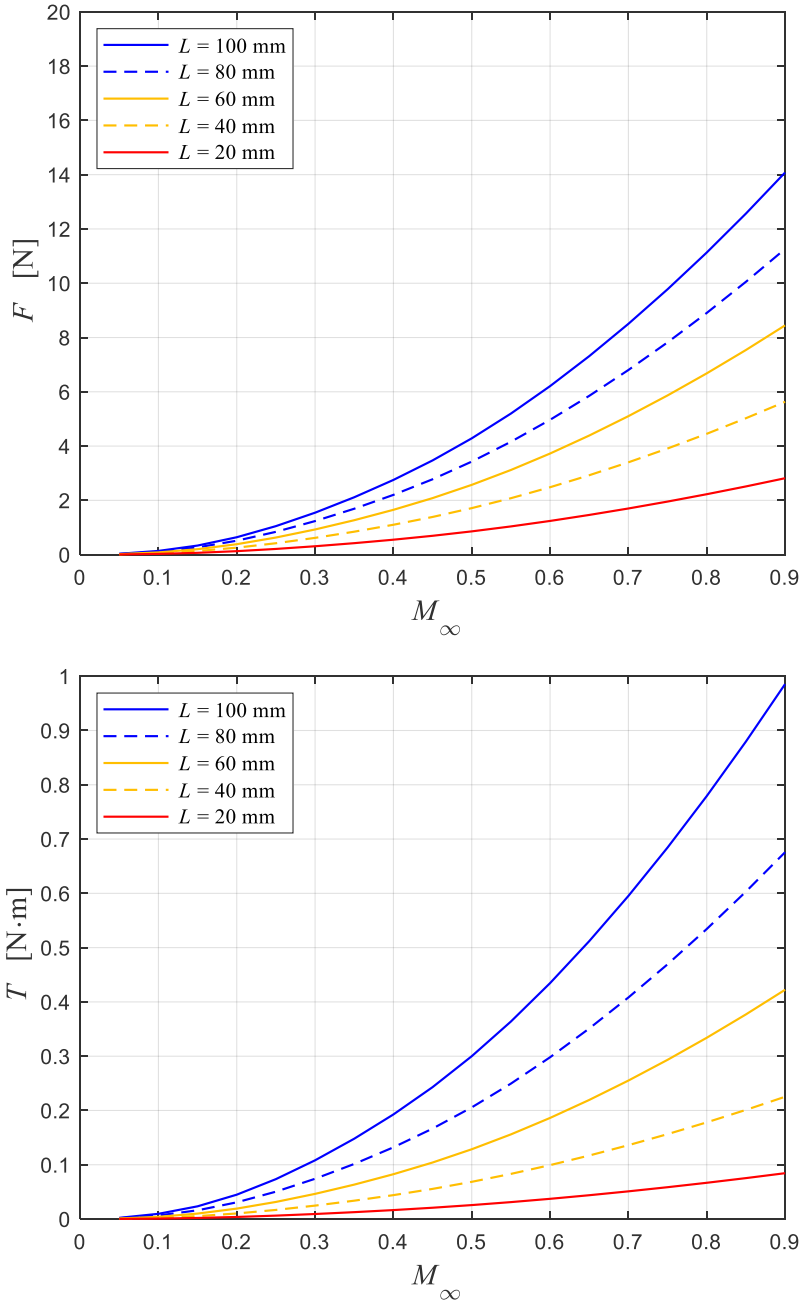

Fig. 4 Predicted force (top) and moment (bottom) at the transducer for a probe with circular shaft of radius r = 1 mm inserted in the 20 mm-thick base for different values of the shaft length L and of the freestream Mach number M_∞.

Figure 4 shows the magnitude F of the force and T of the moment at the top of the transducer predicted using Eqs. 1, 2 and 5 for a probe with circular shaft of radius r = 1 mm inserted in the 20 mm-thick base for different values of the shaft length L and of the freestream Mach number M_∞. The moment predicted for using a 100 mm-long probe at Mach 0.9 is close to the maximum value measurable by the transducer. To avoid saturation of the signal and potential overload of the transducer, an 80 mm-long probe was selected for fabrication and testing for which the predicted largest force and moment are slightly higher than 1/2 and 2/3 of the corresponding maximum measurable values, Fig. 4. Since the moment spans a larger portion of the measurable range, it should provide a better resolution of the velocity and the direction of the flow acting on the probe.

Using Eqs. 3 and 4, the displacement δ of the tip of the selected probe was found to reach 4.5 mm at Mach 0.9. This value is less than 6% of the shaft length and indicates that, different from the more flexible polystyrene probe tested at low velocity [26], this probe only moderately bends in the direction of the freestream.

Figure 5 details the components of the aero-whisker fabricated for the flow measurements in the transonic wind tunnel of the Aeromechanical Systems Group (ASG) of Cranfield University. This an ejector-driven tunnel with a 229 mm-wide and 205 mm-high test section. Although the tunnel was designed primarily for measurements at high subsonic and transonic flow conditions, the flow in its test section can be manually adjusted to achieve Mach numbers as low as Mach 0.15.

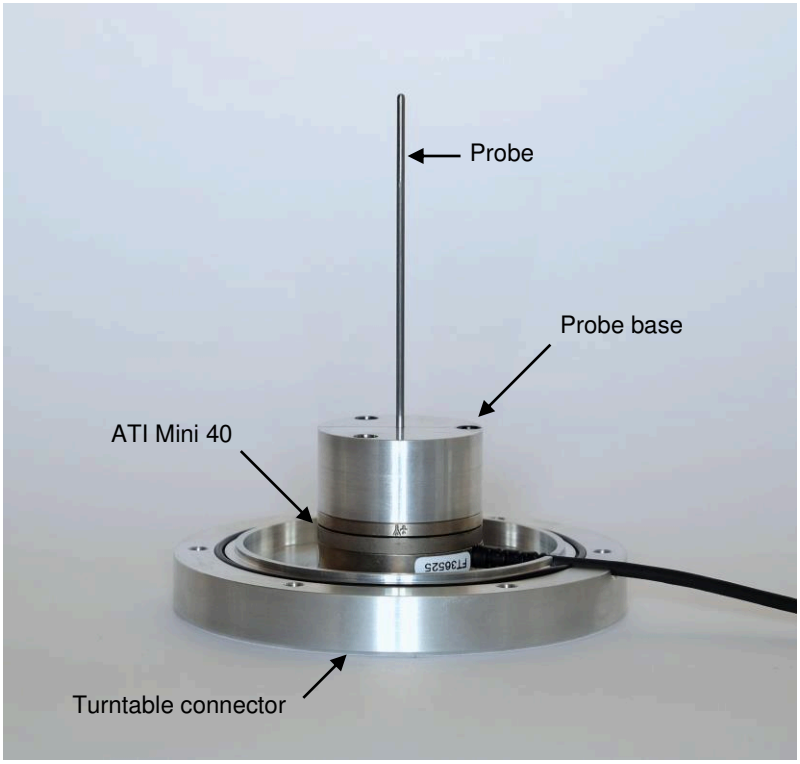

Fig. 5 Components of the aero-whisker fabricated for flow measurements in the ASG transonic wind tunnel.

The aero-whisker was installed in a turntable placed on left-side wall of the wind-tunnel test section, Fig. 6. The turntable allowed full 360° rotation with reference markings at 1° increments. Measurements were made at freestream Mach numbers from 0.15 to 0.87 measured with a pitot-static probe protruding 107 mm into the freestream from the opposite side wall in a position clear of the aero-whisker and its wake. The total temperature was measured by a thermocouple located in the plenum upstream of the contraction to the test section. This together with the total and static pressure from the pitot-static probe allowed calculating the other characteristics of the freestream. The corresponding Reynolds number based on the shaft's diameter ranged from $0.67 \cdot 10^4$ to $2.85 \cdot 10^4$.

The local thickness of the boundary layer at the highest Mach number was 8 mm. For selected Mach numbers, measurements were recorded by changing the turntable-set angle θ_∞ of the freestream relative to the probe from -88° to +88° with 10° increments (8° between ±88° and ±80°). Measurements were not made at θ_∞ = ±90° since the alignment of the x axis of the transducer relative to the centerline of the test section could only be set within an estimated ±2.0°.

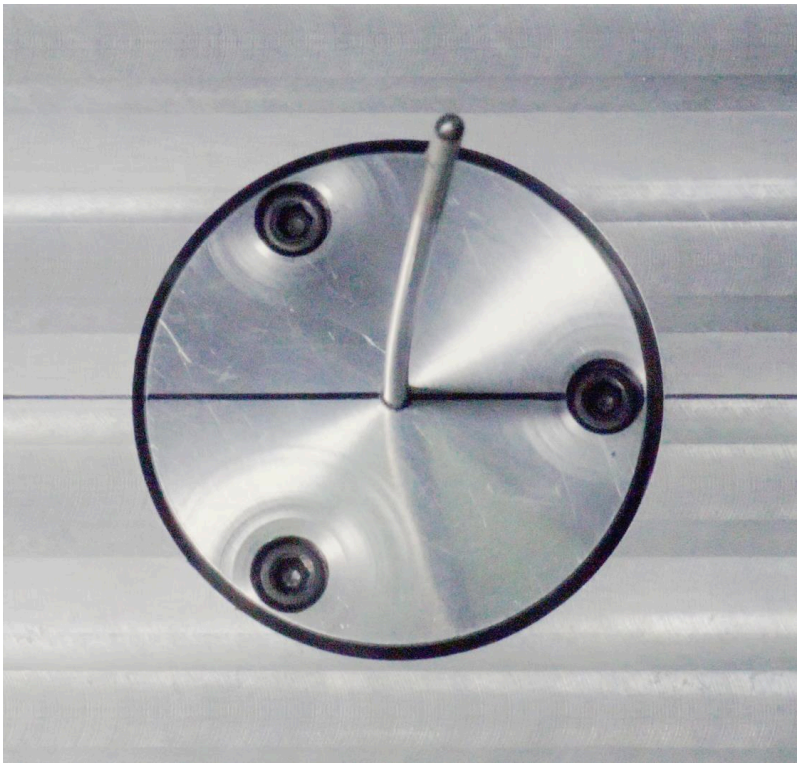

Fig. 6 Aero-whisker in a Mach 0.85 flow inside the ASG transonic wind tunnel.

V. Results

The signals of the components of the moment along the x and y axes of the transducer were acquired for 1 second at a sampling frequency of 1 kHz. The mean value of the samples was used to obtain the average components T_x and T_y during the acquisition time. The magnitude of the moment T was then obtained as:

$$T = \sqrt{T_x^2 + T_y^2} \tag{6}$$

Figure 7 shows how the magnitude T of the moment measured by the transducer changes with the freestream Mach number M_∞. Circles indicate the experimental data whose values are somewhat lower than those, repeated from Fig. 4, predicted in the design of the 80 mm-long probe. At Mach numbers above 0.7 the magnitude of the moment starts following a lower trend with increasing the freestream Mach number.

Wind-tunnel measurements by Knowder and Pruden [28] and Matt [29] and flight tests by Welsh [30] indicated a dip of the cylinder drag coefficient as the freestream Mach number increases above about 0.7 to 0.8. Macha showed that this dip is caused by compressibility effects [31]. Figure 8 compares the drag coefficient of the shaft with $L/2r$ = 40 from the current wind-tunnel measurements with the drag coefficient of cylinders with $L/2r$ = 30 from flight tests [30] and confirms that the aero-whisker probe experiences a drag-coefficient dip at freestream Mach numbers higher than 0.75. This dip lessens the increase of the shaft's drag with the freestream Mach number and thus the corresponding moment measured by the transducer, Fig. 7. Accordingly, we divide the freestream Mach range of the current measurements in two subranges: the first comprising Mach numbers up to M_{12} = 0.75

corresponding to the onset of the drag-coefficient dip, Fig. 8, and the second comprising Mach numbers higher than M_{12}. Denser measurements were taken in the second subrange to clearly resolve the local trend of the magnitude of the moment.

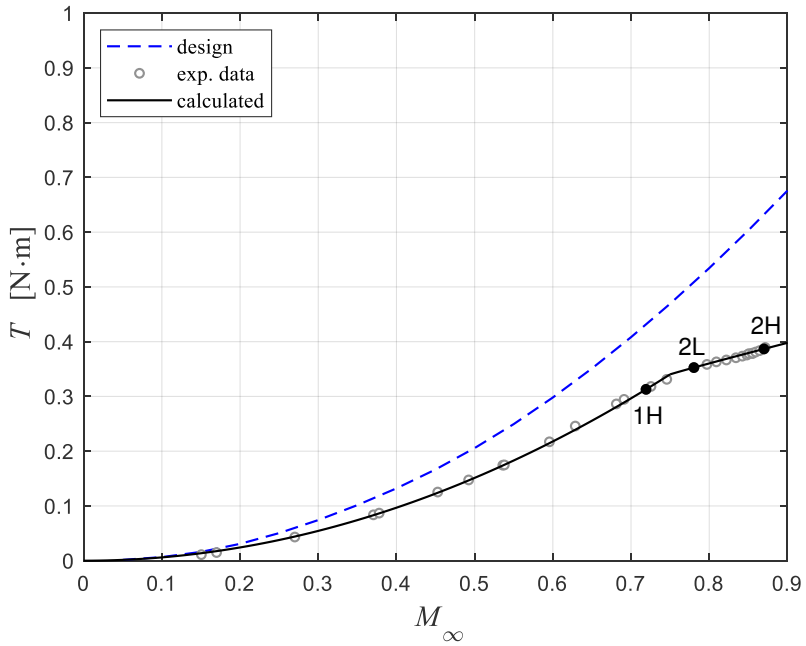

Fig. 7 Magnitude of the moment predicted in the design of the 80 mm-long probe, measured experimentally and calculated based on the experimental data for different values of the freestream Mach number.

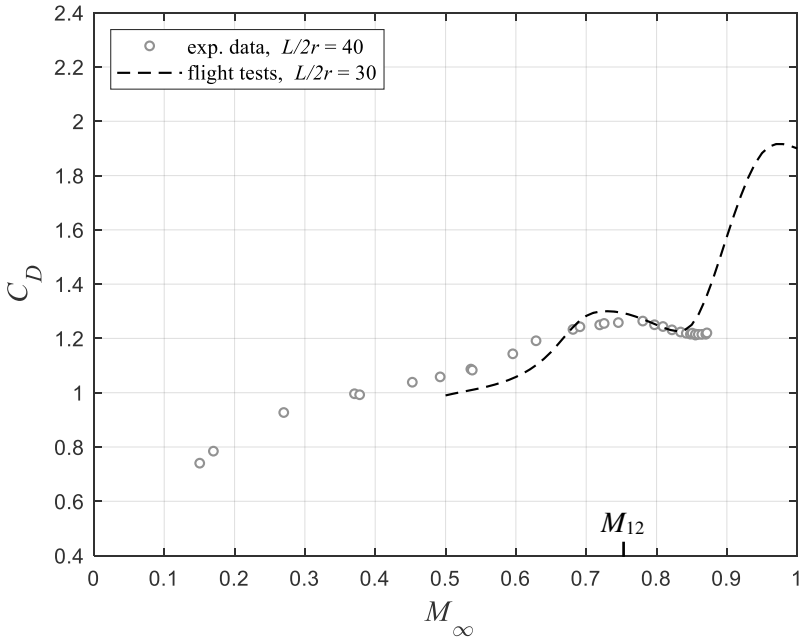

Fig. 8 Drag coefficient of the shaft with $L/2r$ = 40 from current wind-tunnel measurements and of cylinders with $L/2r$ = 30 from flight tests [30].

Since, except at the lower freestream Mach and Reynolds numbers, the shaft has a drag coefficient of about 1.2, Fig. 8 and Fig. 3, and it bends little in the flow [32], we can assume that Eq. 5 is fundamentally a function of M_∞^2. Thus, the function describing the increase of T with M_∞ in the first subrange has form:

$$T = k_1 \cdot M_\infty^2 \tag{7}$$

for which the coefficient k_1 can be calculated as:

$$k_1 = \frac{T_{1\mathrm{H}}}{M_{1\mathrm{H}}^2} \tag{8}$$

where $T_{1\mathrm{H}}$ is the value of T at a freestream Mach number $M_{1\mathrm{H}}$ close to M_{12}. The coefficient $k_1 = 0.605$ was found using the experimental datum $M_{1\mathrm{H}} = 0.719$ with $T_{1\mathrm{H}} = 0.313$, marked as a black circle in Fig. 7. By using Eq. 7, the value of T_{12} corresponding to M_{12} was then found to be 0.340.

A quadratic-Mach-number law did not fit well the data in the second subrange. By allowing the exponent of M_∞ to assume any value b_2, the increase of T with M_∞ in the second subrange takes the form:

$$(T - T_{12}) = k_2 \cdot (M_\infty - M_{12})^{b_2} \tag{9}$$

for which the exponent b_2 and the coefficient k_2 can be calculated as:

$$b_2 = \frac{\log\left(\frac{T_{2\mathrm{H}} - T_{12}}{T_{2\mathrm{L}} - T_{12}}\right)}{\log\left(\frac{M_{2\mathrm{H}} - M_{12}}{M_{2\mathrm{L}} - M_{12}}\right)} \tag{10}$$

$$k_2 = \frac{T_{2\mathrm{H}} - T_{12}}{(M_{2\mathrm{H}} - M_{12})^{b_2}} \tag{11}$$

where $T_{2\mathrm{L}}$ and $T_{2\mathrm{H}}$ are the values of T at two suitably-spaced Mach numbers $M_{2\mathrm{L}}$ and $M_{2\mathrm{H}}$ higher than M_{12}. The exponent $b_2 = 0.923$, almost a linear law, and the coefficient $k_2 = 0.357$ were found using the experimental data $M_{2\mathrm{L}} = 0.780$ with $T_{2\mathrm{L}} = 0.353$ and $M_{2\mathrm{H}} = 0.870$ with $T_{2\mathrm{H}} = 0.387$, marked as black circles in Fig. 7.

The increase of T with M_∞ calculated as indicated above is shown in Fig. 7 as a black line passing through the experimental data. The inverse function:

$$M = \left(\frac{T}{k_1}\right)^{1/2} \qquad \text{for } T \le T_{12} \tag{12a}$$

$$M = \left(\frac{T - T_{12}}{k_2}\right)^{1/b_2} + M_{12} \qquad \text{for } T > T_{12} \tag{12b}$$

can then be used to calculate the Mach number M measured by the aero-whisker from the magnitude T of the moment measured by its transducer. This represents the calibration curve of the aero-whisker which is shown in Fig. 9 together with the experimental data.

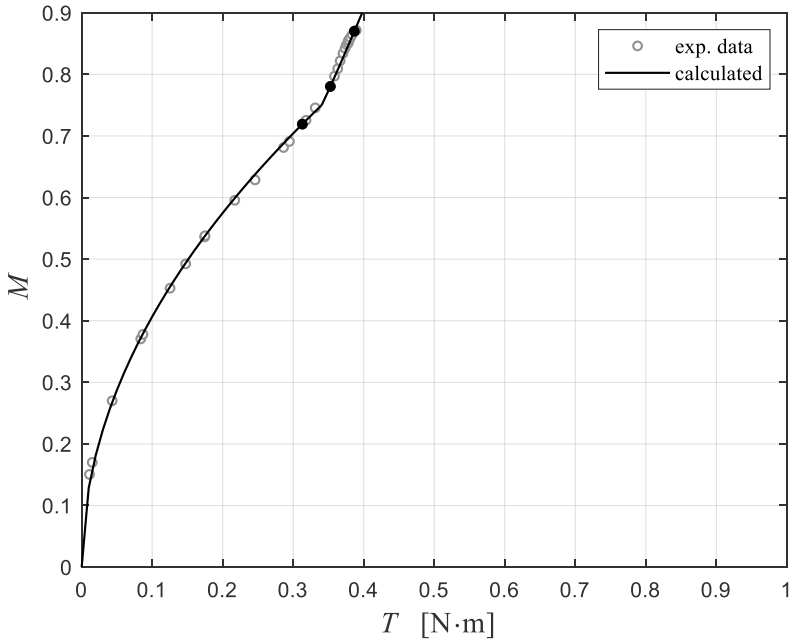

Fig. 9 Mach number measured by the aero-whisker as a function of the magnitude of the moment measured by its transducer.

Angular measurements were recorded at nominal values of M_∞ = 0.59, 0.69, 0.77 and 0.85 by changing the turntable-set angle θ_∞ of the freestream relative to the probe from -88° to +88°. Figure 10 verifies that these measurements are consistent with those discussed above by comparing the magnitude of the moment at different angles, shown as colored circles, with the increase of T with M_∞ calculated using Eqs. 7 and 9. The actual Mach number of each angular measurements is in the neighborhood of its nominal value with a spread becoming larger at lower Mach numbers for which the manual control of the flow conditions was more difficult. Because of this, angular measurements were not taken for M_∞ < 0.59.

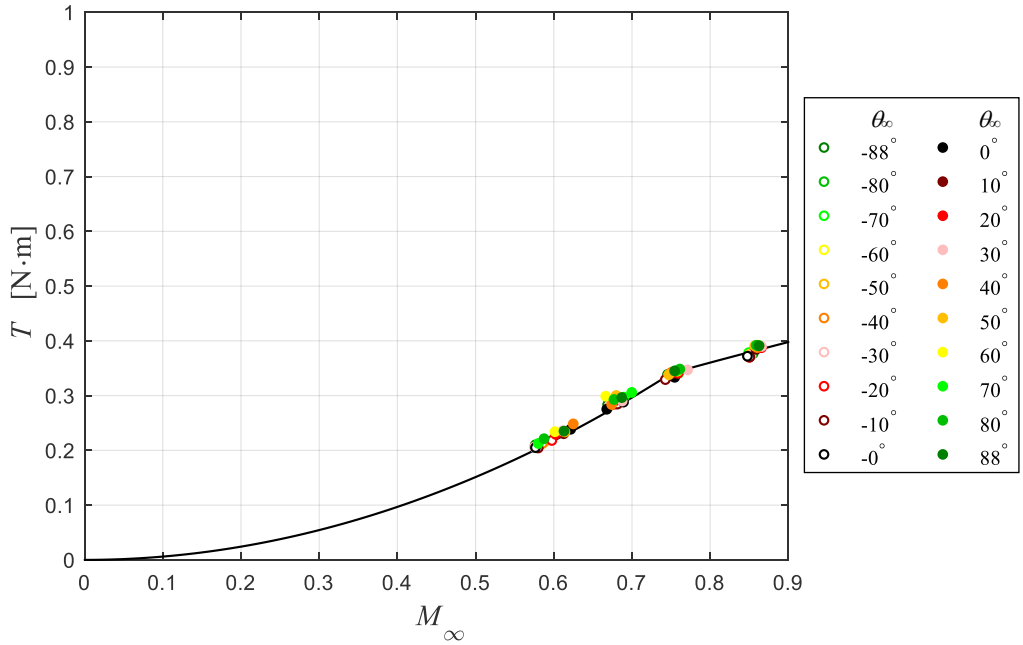

Fig. 10 Magnitude of the moment measured with changing the angle θ_∞ of the freestream relative to the probe at selected Mach numbers (circles) and calculated using Eqs. 7 and 9 over a larger Mach range (line).

The angle θ of the flow measured by the aero-whisker was obtained from T_x and T_y as:

$$\theta = \tan^{-1}\left(\frac{T_x}{T_y}\right) \tag{14}$$

Figure 11 shows that the angle θ of the flow measured by the aero-whisker closely match the true angle θ_∞ of the freestream relative to the aero-whisker probe.

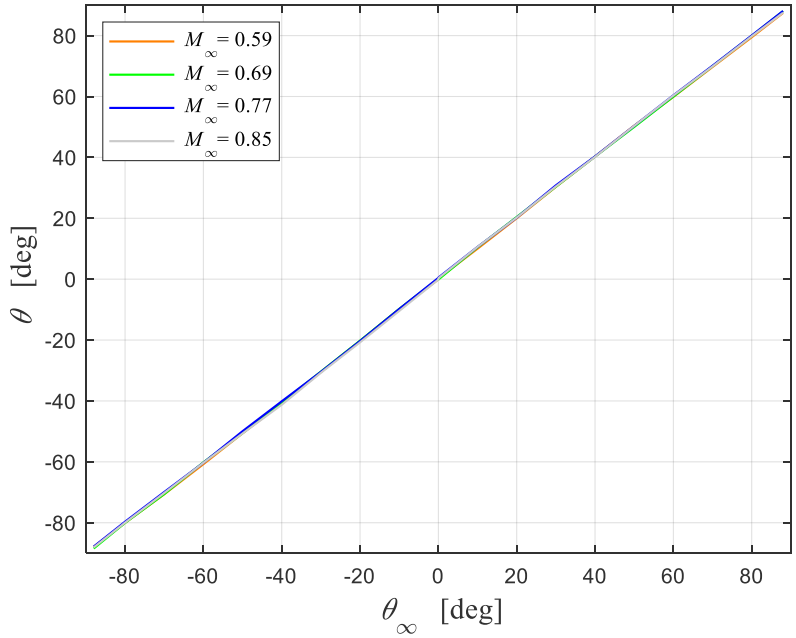

Fig. 11 Comparison of the angle of the flow measured by the aero-whisker with the angle of the freestream relative to its probe.

Small vibrations of the probe in the flow were observed and an analysis was performed to check if these would affect the results discussed above.

The probe's shaft is a long cylinder in a cross flow. Accordingly, vortex shedding past the shaft could lead to periodic vortex-induced vibration (VIV) of the probe. The proximity (indicatively within 10%) of the VIV frequency to that of the dominant vibration mode of the probe could excite resonant oscillations affecting the values measured by the transducer.

The frequency of the dominant vibration mode of the probe and transducer was obtained by displacing the shaft in still air and releasing it to oscillate along the x and y axes. Timetraces $T_y(t)$ and $T_x(t)$ of the components of the moment measured along the transducer's axes normal to the direction of oscillation were acquired at a sampling frequency of 10 kHz. Each timetrace was low-pass filtered at 4.9 kHz by a Butterworth filter to avoid aliasing and its narrowband power spectrum was computed using a 5000-point short-time Fourier transform providing a spectral resolution of 2 Hz. The spectra in both the x and y directions showed a strong peak at about 170 Hz corresponding to the dominant vibration mode of the probe and transducer. This frequency recast as Strouhal number in the Mach number range of the experimental data spans from $2{\cdot}10^{-2}$ to $1{\cdot}10^{-3}$. At the matching Reynolds number these values are significantly lower than the VIV Strouhal numbers from 0.21 to 0.19 [33] of an infinite-length, circular cylinder which is assumed to approximate well the VIV characteristics of the $L/2r = 40$ shaft. This indicates that the vortices shed by the probe's shaft should not excite resonant oscillations of the probe and the transducer.

The impact of the observed small vibrations was also assessed by evaluating their magnitude relative to the displacement induced by the drag. To this aim the oscillating components $T(t) - T$ of the moment magnitude about the steady component T, Eq. 6, were normalized by T itself. The corresponding timetraces were low-pass filtered at

499 Hz by a Butterworth filter to avoid aliasing, their narrowband power spectra were computed using a 500-point short-time Fourier transform providing a spectral resolution of 2 Hz and the results were converted to decibels.

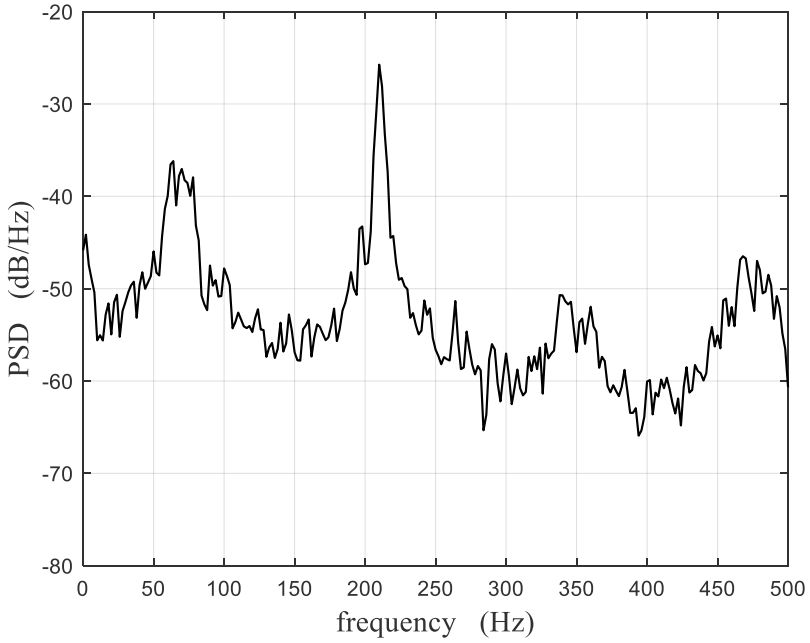

Fig. 12 Power spectral density of the oscillating components relative to the steady component of the moment magnitude measured at M_∞ = 0.371.

The power spectral density of the oscillating components relative to the steady component of the moment magnitude measured at the freestream Mach number 0.371 is shown in Fig. 12. The highest peak of -26 dB at 210 Hz indicates that the magnitude of the largest vibratory component of the moment is about 400 times smaller than the steady component which represents the overall drag effect. Similar spectra with lower values were obtained for all the other measurements shown in Fig. 7.

The analysis above suggests that the vibrations of the probe in the freestream do not affect the measurement of the velocity and direction of the flow by this aero-whisker configuration and that its probe's shaft does not require vortex-shedding suppressors.

VI. Conclusion

An aero-whisker was developed and tested that can be used to measure the velocity and the direction of a subsonic flow in which it protrudes. The probe of the aero-whisker is a circular shaft longer than the local thickness of the boundary layer and supported by a base. The probe is connected to a torque transducer placed at its base that measures the moment induced by the drag of the probe immersed in the flow. A prototype aero-whisker was designed and fabricated for testing the concept in a high-speed wind tunnel. Measurements were made with the probe in the freestream at Mach numbers from 0.15 to 0.87 and angles relative to the probe from -88° to +88°. The drag coefficient of the aero-whisker was found to slightly decrease at Mach numbers higher than 0.75 which is consistent with the drag of circular cylinders in high-speed crossflows and is caused by compressibility effects. With a calibration that accounts for this phenomenon, the aero-whisker was able to accurately measure the Mach number and the direction of the freestream. This performance was not affected by small vibrations of the probe in the flow. Further research on aero-whiskers for aircraft applications can explore: flight-testing the concept on an aircraft; optimizing the probe's shape and materials to obtain desirable bending characteristics in the freestream; study how the data from multiple aero-whiskers in a distributed sensor configuration can fuse with those from traditional air data probes and create fault-tolerant systems.

References

[1] Bureau d'Enquêtes et d'Analyses pour la sécurité de l'aviation civile (BEA), "Final Report On the accident on 1st June 2009 to the Airbus A330-203 registered F-GZCP operated by Air France flight AF 447 Rio de Janeiro - Paris," Jul. 2012.

[2] Komite Nasional Kaselamatan Transportasi Republic of Indonesia, "Aircraft Accident Investigation Report PT. Lion Mentari Airlines Boeing 737-8 (MAX); PK-LQP Tanjung Karawang, West Java Republic of Indonesia 29 October 2018," Final report KNKT.18.10.35.04, Oct. 2019.

[3] The Federal Democratic Republic of Ethiopia, Ministry of Transport and Logistics, Aircraft Accident Investigation Bureau, "Investigation Report on Accident to the B737-MAX8 Reg. ET-AVJ operated by Ethiopian Airlines 10 March, 2019," Report No. AI-01/19, 23 Dec. 2022.

[4] National Transportation Safety Board, "US Comments on Draft Aircraft Accident Investigation Report Ethiopian Airlines Flight 302 Boeing 737-8 MAX, ET-AVJ Ejere, Ethiopia March 10, 2019," 27 Dec. 2022.

[5] Bureau d'Enquêtes et d'Analyses pour la sécurité de l'aviation civile (BEA) "BEA main comments on the draft Final Report for the accident that occurred on 10th March 2019 to the Boeing 737-8 MAX registered ET-AVJ operated by Ethiopian Airlines," Dec. 2022.

[6] Sterbing-D'Angelo, S., Chadha, M., Chiu, C., Falk, B., Xian, W., Barcelo, J., Zook, J. M., and Moss, C. F., "Bat wing sensors support flight control," *Proceedings National Academy of Science USA*, Vol. 108, No. 27, Jun. 2011, pp. 11291-11296.
doi: 10.1073/pnas.1018740108

[7] Jiang, Y., Zhao, P., Ma, Z., Shen, D., Liu, G., and Zhang, D., "Enhanced flow sensing with interfacial microstructures," *Biosurface and Biotribology*, Vol. 26, No. 1, Feb. 2020, pp. 12-19.
doi: 10.1049/bsbt.2019.0043

[8] Maschmann, M. R., Ehlert, G. J., Dickinson, B. T., Phillips, D. M., Ray, C. W., Reich, G. W., and Baur, J. W., "Bioinspired carbon nanotube fuzzy fiber hair sensor for air-flow detection," *Advanced Materials*, Vol. 26, No. 20, Mar. 2014, pp. 3230-3234.
doi: 10.1002/adma.201305285

[9] Slinker, K., Kondash, C., Dickinson, B. T., and Baur, J. W., "High-Bandwidth and Sensitive Air Flow Sensing Based on Resonance Properties of CNT-on-Fiber Hairs," *Journal of Carbon Research*, Vol. 3, No. 1, Mar. 2017, 6.
doi: 10.3390/c3010006

[10] Bian, Y., Zhang, Y., and Xia, X., "Design and Fabrication of a Multi-electrode Metal-core Piezoelectric Fiber and Its Application as an Airflow Sensor," *Journal of Bionic Engineering*, Vol. 13, Sep. 2016, pp. 416-425.
doi: 10.1016/S1672-6529(16)60314-1

[11] Jiang, Y., Shen, D., Liu, M., Ma, Z., Zhao, P., Feng, L., and Zhang, D., "Fabrication of graphene/polyimide nanocomposite-based hair-like airflow sensor via direct inkjet printing and electrical breakdown," *Smart Materials & Structures*, Vol. 28, May 2019, 065028.
doi: 10.1088/1361-665X/ab18cb

[12] Wang, Y. H., Lee, C. Y., and Chiang, C. M., "A MEMS-based air flow sensor with a free-standing micro-cantilever structure," *Sensors*, Vol. 7, Oct. 2007, pp. 2389-2401.
doi: 10.3390/s7102389

[13] Sadeghi, M. M., Peterson, R. L., and Najafi, K., "Micro-hydraulic structure for high performance bio-mimetic air flow sensor arrays," *International Electron Devices Meeting*, Washington, DC, USA, 5-7 Dec. 2011.
doi: 10.1109/IEDM.2011.6131638

[14] Takahashi, H., Isozaki, A., Matsumoto, K., and Shimoyama, I., "A cantilever with comb structure modeled by a bristled wing of thrips for slight air leak," *28th IEEE International Conference on Micro Electro Mechanical Systems (MEMS)*, Estoril, Portugal, 18-22 Jan. 2015, pp. 706-709.
doi: 10.1109/MEMSYS.2015.7051055

[15] Bruecker, C. H., and Mikulich, V., "Sensing of minute airflow motions near walls using pappus-type nature-inspired sensors," *PLoS ONE*, Vol. 12, No. 6, Jun. 2017, 0179253.
doi: 10.1371/journal.pone.0179253

[16] Ma, R. H., Wang, D. A., Hsueh, T. H., and Lee C. H., "A MEMS-Based Flow Rate and Flow Direction Sensing Platform with Integrated Temperature Compensation Scheme," *Sensors*, Vol. 9, Jul. 2009, pp. 5460-5476.
doi: 10.3390/s90705460

[17] Dagamseh, A. M. K., Lammerink, T. S. J., Sanders, R., Wiegerink, R. J., and Krijnen, G. J. M., "Towards high-resolution flow cameras made of artificial hair flow-sensors for flow pattern recognition," *IEEE 24th International Conference on Micro Electro Mechanical Systems (MEMS)*, Cancun, Mexico, 23-27 Jan. 2011.
doi: 10.1109/MEMSYS.2011.5734508

[18] Droogendijk, H., Bruinink, C. M., Sanders, R. G. P., and Krijnen, G. J. M., "Tunable Sensor Response by Voltage-Control in Biomimetic Hair Flow Sensors," *Micromachines*, Vol. 4, Mar. 2013, pp. 116-127.
doi: 10.3390/mi4010116

[19] Casas, J., Steinmann, T., and Krijnen, G., "Why do insects have such a high density of flow-sensing hairs? Insights from the hydromechanics of biomimetic MEMS sensors," *Journal of the Royal Society Interface*, Vol. 7, Apr. 2010, pp. 1487-1495.
doi: 10.1098/rsif.2010.0093

[20] Beem, H., Hildner, M., and Triantafyllou, M., "Characterization of a harbor seal whisker-inspired flow sensor," *IEEE OCEANS 2012 Conference*, 14-19 Oct. 2012.
doi: 10.1109/OCEANS.2012.6404978

[21] Kottapalli, A. G. P., Asadnia, M., Hans, H., Miao, J. M., and Triantafyllou, M. S., "Harbor Seal Inspired MEMS Artificial Micro-Whisker Sensor," *IEEE 27th International Conference on Micro Electro Mechanical Systems (MEMS)*, 26-30 Jan. 2014, pp. 741-744.
doi: 10.1109/MEMSYS.2014.6765747

[22] Beem, H. R., and Triantafyllou, M. S., "Wake-induced 'slaloming' response explains exquisite sensitivity of seal whisker-like sensors," *Journal of Fluid Mechanics*, Vol. 783, Oct. 2015, pp. 306-322.
doi: 10.1017/jfm.2015.513

[23] Zheng, X., Kamat, A. M., Harish, V. S., Cao, M., and Kottapalli, A. G. P., "Optimizing Harbor Seal Whisker Morphology for Developing 3D-Printed Flow Sensor," *21st International Conference on Solid-State Sensors, Actuators and Microsystems (Transducers)*, 20-24 Jun. 2021.
doi: 10.1109/Transducers50396.2021.9495504

[24] Wood, K. T., Araujo-Estrada S., Richardson, T., and Windsor, S., "Distributed Pressure Sensing-Based Flight Control for Small Fixed-Wing Unmanned Aerial Systems," *Journal of Aircraft*, Vol. 56, No. 5, Sep.-Oct. 2019, pp. 1951-1960.
doi: 10.2514/1.C035416

[25] Araujo-Estrada, S. A., and Windsor, S. P., "Aerodynamic Variables and Loads Estimation Using Bio-Inspired Distributed Sensing," AIAA Paper 2019-1934, Jan. 2019.

[26] Debiasi, M., Finnis, M., and Galvao Wall, D., "Aero-whisker for Aircraft Flow Sensing," Royal Aeronautical Society Applied Aerodynamics Conference, London, United Kingdom, 13-15 Sep. 2022.

[27] Anderson, J. D. Jr. *Fundamentals of Aerodynamics*, 2nd ed., McGraw Hill, 1991.
ISBN 0-07-001679-8.

[28] Knower, A. E. and Pruden, F. W., "On the Drag of Circular Cylinders at High Speed," British Aeronautics Research Council, R&M No. 1933, 1944.

[29] Matt, H., "Measurement of Drag of Round Rods of Various Diameters at High Subsonic Airspeed," Deutsche Luftfahrtforschung, Forschungsberichte (Report) No. 1825, 1943; results also reported by Naumann, A. and Pfeifer, H., "Uber Die Grenzschichtstromung am Zylinder bei hohen Geschwindigkeiten," *Advances in Aeronautical Sciences*, Vol. 3, edited by Th. von Karman, Pergamon Press, New York, 1962, pp. 185-206.

[30] Welsh, C. J., "The Drag of Finite Length Cylinders Determined from Flight Tests at High Reynolds Numbers for a Mach Numbers Range from 0.5 to 1.3," NACA TN 2491, Jun. 1973.

[31] Macha, J. M., "Drag of Circular Cylinders at Transonic Mach Numbers," *Journal of Aircraft*, Vol. 14, No. 6, Jun. 1977, pp. 605-607.

[32] Leclercq, T. and de Langre, E., "Drag reduction by elastic reconfiguration of non-uniform beams in non-uniform flows," *Journal of Fluids and Structures*, Vol. 60, Jan. 2016, pp. 114–129. [DOI: 10.1016/j.jfluidstructs.2015.10.007]

[33] White, F. M., *Fluid Mechanics*, 4th ed., McGraw Hill, 1999.
ISBN 0-07-069716-7